"This manuscript has been accepted for publication in Composite Structures. The manuscript will undergo copyediting, typesetting, and review of the resulting proof before it is published in its final form. Please note that during the production process errors may be discovered which could affect the content, and all disclaimers that apply to the journal apply to this manuscript. A definitive version was subsequently published in:
COMPOSITE STRUCTURES, VOL 126, AUGUST 2015, PAGES 329-336
DOI http://dx.doi.org/doi:10.1016/j.compstruct.2015.02.083 "

A numerical study of bioinspired nacre-like composite plates under blast loading

E.A. Flores-Johnson[1,*], Luming Shen[1], Irene Guiamatsia[1], Giang D. Nguyen[2]

[1]School of Civil Engineering, The University of Sydney, Sydney, NSW 2006, Australia
[2]School of Civil, Environmental and Mining Engineering, The University of Adelaide, Adelaide, SA 5005, Australia

Abstract: In this paper, a multi-layered composite inspired by the hierarchical structure of nacre and made of layers of aluminium alloy AA 7075 bonded with toughened epoxy resin is introduced for blast resistant applications. The performance of the proposed nacre-like 3.3-mm and 5.4-mm thick composite plates, made of 1.1-mm thick AA 7075 layers, under localised impulsive loading was numerically studied. The epoxy material was modelled using user-defined interface cohesive elements that properly take into account both strength and toughness enhancements under compression. As compared to bulk plates, the improvement in blast resistance performance was numerically observed in the nacre-like plates, which required larger loads to reach the onset of failure. In addition, a reduction of the peak velocity and maximum deflection of the back face was observed for the nacre-like plates. This improvement is explained by the hierarchical structure facilitating a globalized energy absorption by inter-layer interlocking, delamination and friction.

Keywords: Bioinspired composite; Layered plates; Blast loading; Cohesive Interface; Finite-element simulation.
*Corresponding author. Tel.: +61 2 9351 2113, Fax: +61 2 9351 3343, Email: emmanuel.flores-johnson@sydney.edu.au

1 INTRODUCTION

The design of lightweight materials with energy-absorbing characteristics for blast and impact applications presents a challenge for innovative engineering to address the competing constraints of light weight on one hand, and impact and shock mitigation on the other hand [1, 2]. In this respect, nature is a source of inspiration for design of novel materials and structures that have both of the above characteristics [3, 4]. High-performance lightweight materials such as wood, bone and abalone shells, made of relatively weak and mundane constituents, are the result of evolutionary developments [5-8]. These natural materials deform via several energy-absorbing mechanisms resulting a remarkable combination of stiffness, strength and toughness [9].

Nacre, the iridescent material found in mollusk shells, is a biological material that exhibits outstanding mechanical properties due to its complex hierarchical structure organized over several length scales [9, 10]. Around 95% of nacre is made of aragonite tablets (a brittle mineral), which are surrounded by a soft organic biopolymer that “glues” them together [11]. Remarkably, nacre exhibits a toughness of about 3000 times higher than that of aragonite [12]. This outstanding performance is attributed to the brick arrangement of the structure, the waviness of the tablets and the multiple interfaces between tablets and layers [5, 13-15].

The behaviour and mechanical properties of nacre have been extensively studied [11, 13, 16]; however, the performance of nacre-like engineering composites at the macroscale (millimetre-size) has only been scarcely explored [9, 12, 14, 17, 18]. Some recent work have shown the strong potential of nacre-like structures with respect to performance in sustaining blast and impact loading when compared to traditional laminated composite plates or bulk plates. Tran et al. [19] showed that a bioinspired composite square plate based on the nacre structure could be used to improve the blast performance of glass fibre/vinylester resin composites subjected to underwater impulsive loading. They found that the bioinspired composite structure helps to relieve the stress concentration by spreading out the induced damages over a larger area. They achieved this by introducing layer waviness to one of the in-plane directions with a triangular wave function [19]. Knipprath et al. [17] showed that the ballistic performance of boron carbide layered plates can be improved by using a simplified nacre-like structural design, which delocalised the impact damage. Their numerical model took into account

layer waviness in both in-plane directions and used a triangular wave function [17]. Our recent numerical investigation has also showed that the impact response of aluminium alloy layered plates can be improved by using a nacre-like design, which took into account layer waviness in both in-plane directions using a sinusoidal function [18]. We demonstrated that the nacre-like design induced a more diffused and globalised damage when compared to monolithic plates.

Based on previous work on bioinspired nacre-like composites, we present numerical analyses to gain a better understanding of the mechanical behaviour of nacre-like aluminium composites with waviness similar to that of the natural nacre material under blast loading. The waviness is taken into account by using a sinusoidal function in both in-plane directions. Nacre-like plates made of 1.1-mm thick aluminium alloy (AA) 7075 layers glued with toughened epoxy resin are subjected to localised impulsive loading. The epoxy material was modelled using a user-defined cohesive element taking into account the increase in both strength and toughness when the debonding occurs under transverse interface compression, together with frictional effects after full debonding. Nacre-like composite plates with thicknesses of 3.3 mm and 5.4 mm were modelled and their blast performance was compared with that of bulk plates of the same thickness. The finite-element model is described in Section 2. Numerical results are presented and discussed in Section 3 followed by conclusions.

2 FINITE ELEMENT MODELLING OF BLAST LOADING OF NACRE-LIKE PLATES

2.1 Problem description

To investigate the blast behaviour of nacre-like composite plates made of AA7075 layers, multi-layered targets consisting of 3 and 5 layers, inspired by the structure of nacre, were made from alternate layers of 1.2-mm and 0.9-mm thickness, glued with toughened epoxy resin (Fig. 1). The geometry of the plates was 200 mm × 200 mm with total thickness of 3.3- and 5.4-mm, for nacre-like plates consisting of 3 and 5 layers, respectively. The waviness of the layers, resembling in the natural nacre material [13], was generated using a sinusoidal function with a wavelength of 20 mm and amplitude of 0.1 mm (Fig. 1(c)). In the natural nacre material, each layer is made of several individual tablets; however, we employ continuous layers in this work since our preliminary analyses showed that discontinuous layers made with tablets were not suitable for resisting localised blast loading. The solid geometry of the model was generated using the computer-aided design software SolidWorks 2012 (Dassault Systemes, SolidWorks Corp., France) and then imported into Abaqus/Explicit (Version 6.11) [20] for pre- and post-processing. The bioinspired composite plates are designed ensuring the preservation of mass when compared to the bulk plates of same thickness. In the simulation, the plates were fully clamped at all of the edge boundaries.

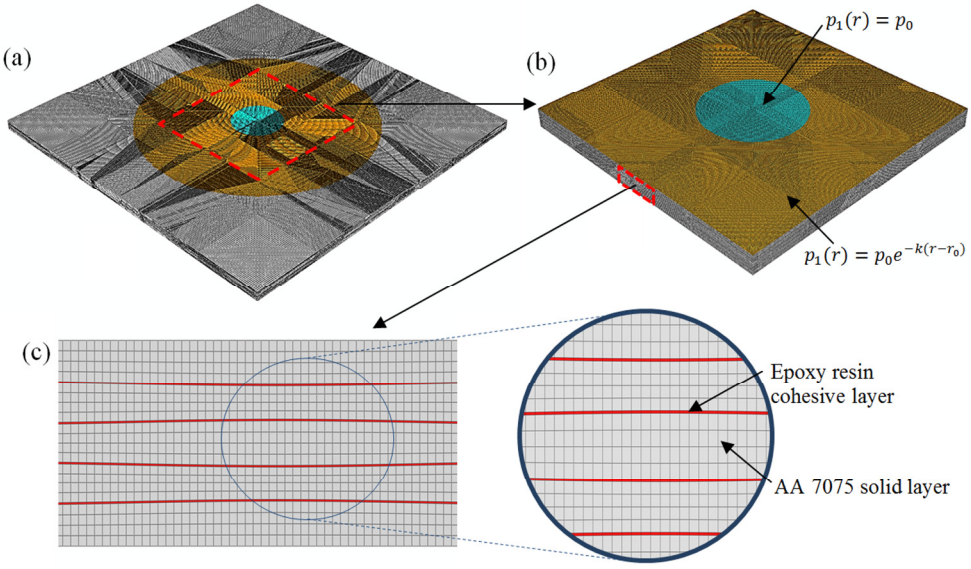

Fig. 1 (a) Finite-element mesh of 5-layer nacre-like plate, (b) closed-up view of central region, (c) cross-section mesh of 5-layer nacre-like plate.

2.2 Materials models

To model the constitutive behaviour of the aluminium layers, the Johnson-Cook material model [21] was used together with the Johnson-Cook fracture criterion [22]. For the cohesive interface between layers, a user-defined cohesive element with compression-enhanced traction separation law [23] was used. Since these material models have been fully described in previous publications [18, 23-25], we therefore refer the reader to these papers for full details.

Aluminium alloy 7075-T651 was used for the layers. The parameters for this material were taken from [26-28] and are shown in Table 1. To model the interface between layers, toughened epoxy adhesive Betamate 1044 was used (Table 2). The parameters in Table 2 for properties of the epoxy resin are identical to those required for standard cohesive elements (COH3D8) in Abaqus (i.e. stiffness, strength, and fracture energies)[20] and were obtained from Wang et al. [29]. There are also additional parameters in Table 2 used in the user-defined cohesive element, explained in detail in our previous papers [18, 23]. They are elastic modulii E and G, tensile strength t_n and shear strength t_s, and fracture energies G_{Ic} and G_{IIc}. The cohesive interface stiffnesses K_n and K_s in this case are E/t_i and G/t_i, respectively, with interface thickness t_i equal to 0.05mm in this study. In addition, the model requires the compressive shear stiffness K_s^f of the fully debonded interface, which is taken to be two to three orders of magnitude less than the initial shear stiffness K_s (in this case K_s^f is equal to $2G_I/1000/t_i$), and the coefficient of friction μ, which is assigned the common value of 0.2 [23].

2.3 Blast loading conditions

To simulate the blast load, a localised impulsive loading that approximates the pressure distribution generated by an explosive disc located at the centre of the plate at a close-range distance is employed as shown in Fig. 2 [30, 31]. The time-dependent non-uniform impulsive load was applied using the following function [32, 33]:

$$P(r,t) = P_1(r)P_2(t) \tag{1}$$

$$P_1(r) = \begin{cases} p_0 & r \le r_0 \\ p_0 e^{-k(r-r_0)} & r_0 < r \le r_b \\ 0 & r > r_b \end{cases} \tag{2}$$

$$P_2(t) = e^{-2t/t_0} \tag{3}$$

where r is the radial distance from the centre of the plate, t is the time, p_0 is the peak pressure, k is the exponential decay constant, r_0 is the radius of the explosive disc, $r_b < L/2$ is a radial distance from the centre of the plate, L is the length of the plate and t_0 is the characteristic decay time for the pulse [32]. The total impulse is defined as:

$$I = 2\pi \int_0^\infty \int_0^{r_b} P(r,t)\,dr\,dt \tag{4}$$

The blast parameters used in this study are shown in Table 3 and were taken from [32]. In the regions of the top surface subjected to non-uniform blast load (Fig. 1(a) and 1(b)), the pressure $P_2(r)$ was applied to each element using the *DLOAD option [20].

Table 1 Material properties and Johnson-Cook model parameters for aluminium alloy AA7075-T651 [26-28].

Material properties	
Density ρ (kg/m^3)	2700
Young's modulus E (GPa)	70
Poisson's ratio ν	0.3
Inelastic heat fraction η	0.9
Specific heat C_p (J/kgK)	910
Strain hardening	
A (MPa)	520
B (MPa)	477
N	0.52
Strain rate hardening	
Reference strain rate $\dot{\varepsilon}_0$ (s^{-1})	5x10^{-4}
C	0.001
Temperature softening	
Reference temperature T_r (K)	293
Melting temperature T_m (K)	893
m	1
Damage parameters	
D_1	0.096
D_2	0.049
D_3	-3.465
D_4	0.016
D_5	1.099
u_{pl}^f (mm)	0.0009

Table 2 Material properties and UEL parameters for epoxy resin Betamate 1044 [29].

Material properties	
Density ρ (kg/m^3)	1350
Elastic modulus in the normal direction E (GPa)	3.1
Elastic modulus in the transverse directions G (GPa)	1.55
Maximum normal traction t_n (MPa)	85.5
Maximum shear traction t_s (MPa)	70
Critical energy-release rate mode I G_{Ic} (J/m^2)	1680
Critical energy-release rate mode II G_{IIc} (J/m^2)	3570
UEL parameters	
Mohr-Coulomb coefficient of friction μ	0.2
Compressive shear stiffness K_s^f (MPa/mm)	3.1/0.05

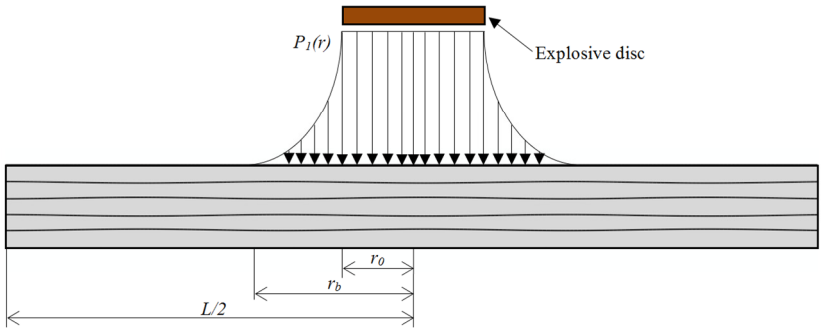

Fig. 2 Blast load spatial distribution.

2.4 Finite element simulation

Finite element models for both nacre-like and bulk plates were constructed and mesh sensitivity analysis was carried out in this Section. Figure 1 shows the 3D finite element mesh of the 5.4-mm thick nacre-like plate, which comprised reduced-integration linear hexahedral elements (C3D8R) for the solid layers, and user-defined elements (UEL) for the cohesive interface between layers (Fig. 1(c)). The cohesive interface was geometrically modelled as a finite-thickness layer. These interface elements are 0.05-mm thick and have shared nodes with the adjacent solid elements. The central area of the plate (40 × 40 mm^2) had an average element size of 0.36×0.36×0.36 mm^3 as illustrated in Fig. 1. The in-plane mesh was then skewed to be coarser towards the edge boundaries. Mesh sensitivity studies showed that this level of refinement was sufficient to obtain a satisfactory converged solution. This is in agreement with the mesh sensitivity studies performed for a similar system [33]. The number of elements for each solid layer and cohesive interface layer were 371712 and 123904, respectively.

A mesh sensitivity analysis was carried out for the 5.4-mm thick bulk plate using a localised pressure pulse of I=7.74 Ns. Three different element sizes were used in the central area (40 × 40 mm^2): 0.27×0.27×0.27 mm^3 (fine mesh), 0.36×0.36×0.36 mm^3 (intermediate mesh), and 0.54×0.54×0.54 mm^3 (coarse mesh), resulting in 20, 15 and 10 through-thickness elements, respectively. Figure 3 shows the predicted maximum deflection and maximum velocity of the plate back face using different numbers of through-thickness elements. The difference between the results with 10 and 20 through-thickness elements is less than 1%. It is noted that if cracking occurs in the back face due to large loads; the crack length could be underestimated for coarser mesh if the analysis is performed beyond certain level of damage. This can be seen in Fig. 4. For a 5.4-mm thick plate under an impulse of I=7.74 Ns, the crack length is similar for the intermediate and small meshes; however, the size of the crack is underestimated for the coarse mesh. Moreover, it is clear from Fig. 4 that the position and shape of the crack converge, as the mesh size is refined. Based on this analysis, an intermediate mesh size of 0.36×0.36×0.36 mm^3 was deemed sufficient for convergence and used throughout in this work to increase the computational efficiency.

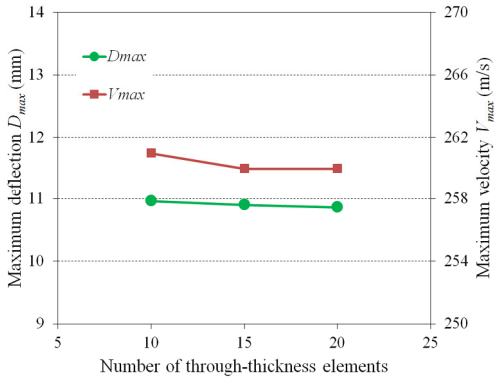

Fig. 3 Predicted maximum deflection and velocity of back face of a 5.4 mm thick bulk plate subjected to an impulsive load of I= 7.74 Ns using different numbers of through-thickness elements.

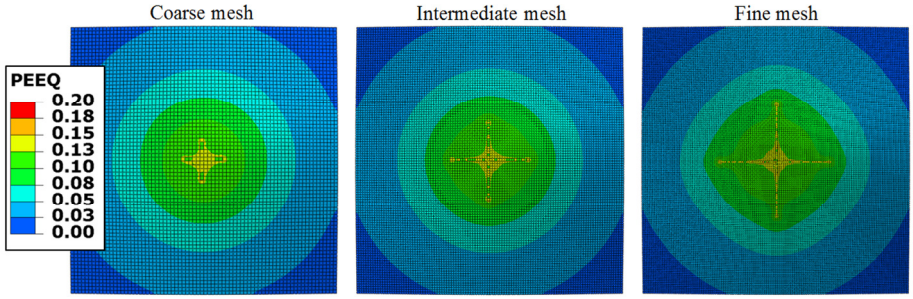

Fig. 4 Predicted crack of back face of a 5.4-mm thick bulk plate subjected to an impulsive load of I= 7.74 Ns using different numbers of through-thickness elements.

3 RESULTS AND DISCUSSION

3.1 Blast performance

Figure 5(a) and 5(b) show the deflection-time histories and velocity-time histories of centre (mid-span) of the back face of the 3.3-mm thick plate subjected to an impulsive load of 4 Ns. It can be seen in Fig. 5(a) that after an initial maximum deflection (t<0.5 ms) the plate deflection starts to oscillate and decreases gradually after each cycle. It is expected that the residual deflection is the average deflection after three more cycles following unloading [34]. Figure 5(b) shows that a peak velocity is reached at t<0.025 ms, which corresponds to the time when most of the loading energy has been transferred to the plate. For this particular case, a significant reduction of the maximum velocity is observed for the nacre-like plate when compared to the bulk plate. Figure 5(c) and 5(d) show the deflection-time histories and velocity-time histories of the centre of the back face of the 5.4-mm thick plate subjected to an impulsive load of 8 Ns. It can be seen in Fig. 5(c) that the deflection of the plate follows a trend similar to that observed in the 3.3-mm thick plate: after an initial maximum peak, the deflection starts to oscillate and reduces gradually with time. Figure 5(d) shows that for the 5.4-mm thick plates the maximum velocity of the nacre-like plate is similar to that of the bulk plate.

Figure 6 plots the maximum deflection D_{max} and maximum velocity V_{max} of the centre of the back face against the magnitude of impulsive loading for different plate configurations and thicknesses. It can be seen that for plate thickness of 3.3 mm, the nacre-like plate performed better by allowing a reduction of 16.6% in D_{max} and 18.1% in V_{max} for an impulsive load of 5 Ns when compared to the bulk plate (crack initiation is observed in the bulk plate in that case). In addition, the nacre-like plate was capable to withstand higher loading (up to 34% higher than that for the bulk plate) before crack initiation was observed in the back face. The advantage of reducing V_{max} is the reduction of kinetic energy of flying fragments that could be generated due to fracture of the back face subjected to localised deformation. For the 5.4-mm thick plates, D_{max} and V_{max} are similar in magnitude for both nacre-like plates and bulk plates until crack initiation is observed in the bulk plate. It was observed that before crack initiation the nacre-like plate could withstand loads up to 29.7% higher than that of the bulk plate. Figure 7 shows the deformation process of 3.3-mm thick bulk and nacre-like plates subjected to an impulsive load of 5 Ns. It can be seen that in the bulk plate (Fig 7(a)), the area of higher magnitude of plastic deformation (PEEQ) is very localized and it accumulates at the mid-span of the back face. This eventually leads to crack initiation. For the nacre-like plate, the area of plastic deformation is more globalised and distributed across the three layers (Fig 7(b)). This can be explained by the fact that for the bulk plate, blast energy is mainly dissipated by bending and plastic deformation while for the nacre-like plate, besides bending and plastic deformation, layers interlocking and delamination also contribute to energy dissipation. The interlocking mechanism due to the layer waviness can be seen in Fig. 8, which shows contour plots of the shear stress in the 3.3-mm thick plates. For the bulk plate (Fig. 8(a)), the shear stress distribution is similar to that of a plate under bending. However, for the nacre-like plate (Fig. 8(b)) shear stress concentrations can be seen along the interfaces due to the layer waviness. This is similar to the stress concentrations found in the natural nacre material subjected to tensile loading [13].

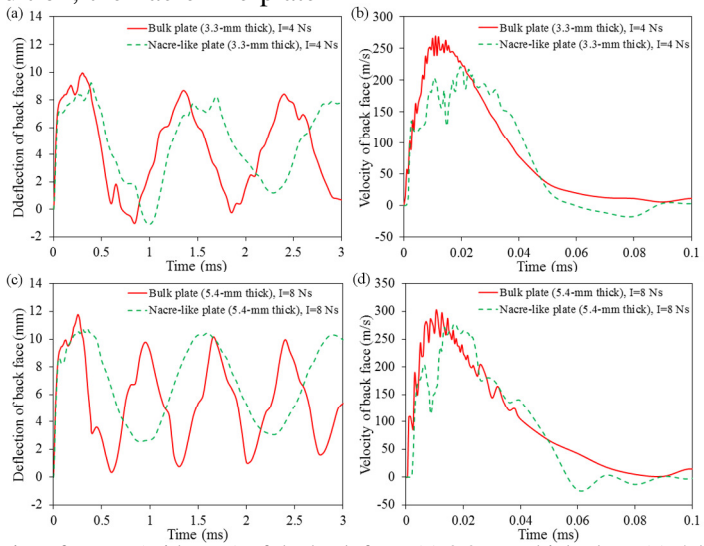

Figure 5 Deflection-time histories of centre (mid-span) of the back face: (a) 3.3-mm thick plate, (c) 5.4-mm thick plate; velocity-time histories of the centre of the back face: (b) 3.3-mm thick plate, (d) 5.4-mm thick plate.

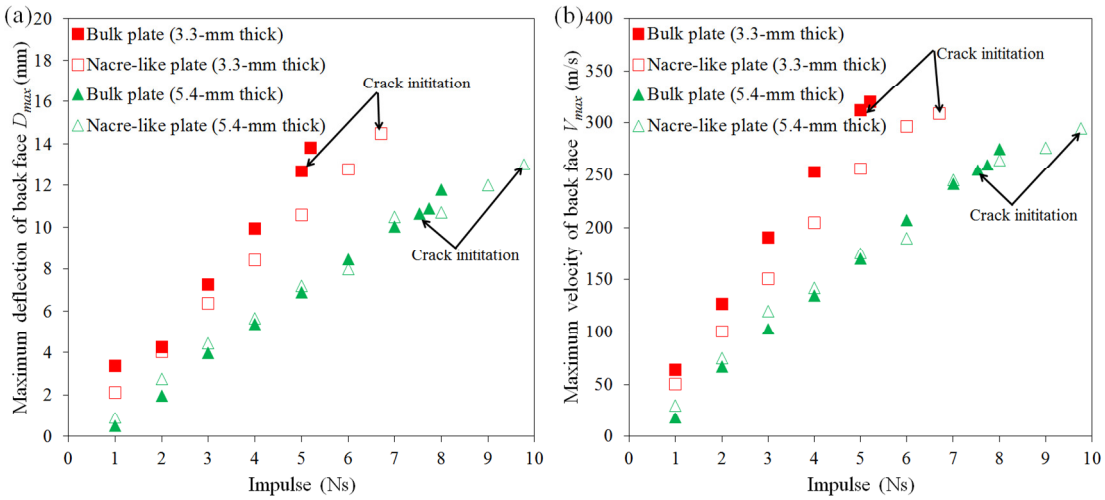

Figure 6 (a) Maximum deflection and (b) maximum velocity of the centre of the back face for various plate configurations and thicknesses with the variation of the total impulsive load.

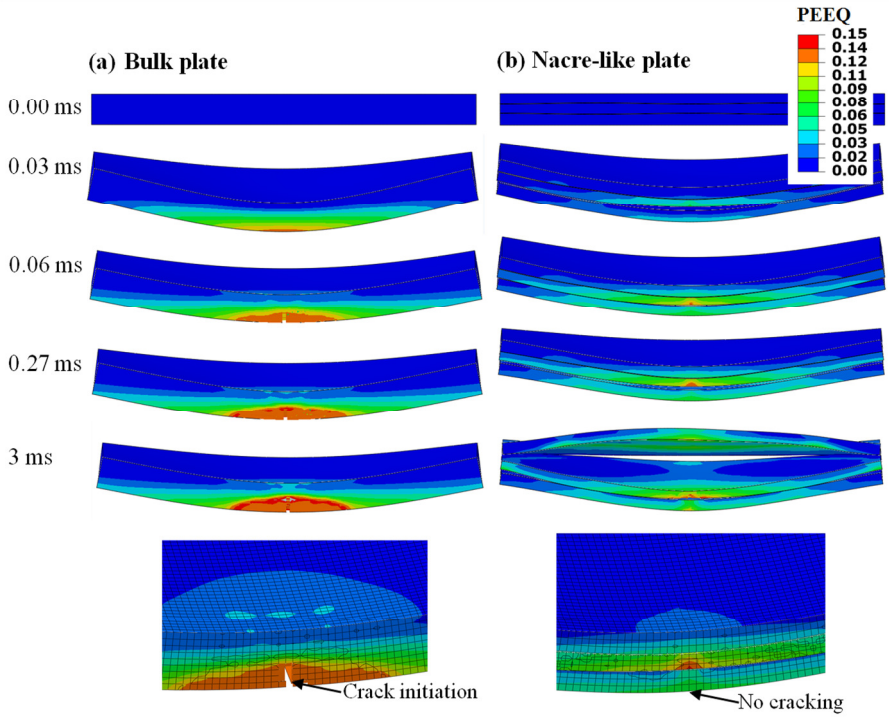

Fig. 7 Deformation process of 3.3-mm thick AA 7075 plates subjected to an impulsive load of 5 Ns: (a) Bulk plate; (b) Nacre-like plate.

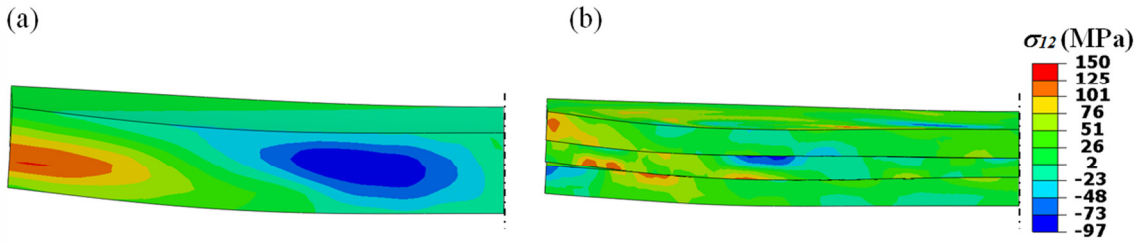

Fig. 8 Contour plots of shear stress σ_{12} in the 3.3-mm thick (a) bulk plate and (b) nacre-like plate at initial stages of blast loading.

Figure 9 shows the deformation process of 5.4-mm thick bulk and nacre-like plates subjected to an impulsive load of 8 Ns. Similarly to the 3.3-mm bulk plate, in the 5.4-mm thick bulk plate plastic deformation is localized at the mid-span of the back face, which eventually leads to crack initiation. For the nacre-like plate, the area of plastic deformation is distributed across five layers and the magnitude of plastic deformation is much lower, due to the fact that part of the blast energy has been dissipated through delamination and then friction between interlocked layers (Fig 9(b)).

The energy imparted by the applied impulsive load to the plates is converted to kinetic and strain energies. Strain energy is either dissipated by plastic deformation, damage and friction or stored in the material [35]. Figure 10 shows time histories of the kinetic and strain energies for the 3.3-mm thick plates (Fig. 10(a)) and 5.4-mm thick plates (Fig. 10(b)). A reduction of the peak kinetic energy is observed for both 3.3-mm and 5.4-mm thick nacre-like plates when compared to their bulk counterparts. This explains the observed lower peak velocities of the centre of the back face in the nacre-like plates. The strain energy at the moment of maximum deflection is smaller for the nacre-like plates than that of the bulk plates. This is explained by the fact that in the nacre-like plates, strain energy is not only dissipated by plastic deformation but also by delamination of layers, followed by friction between them.

The numerical results show that a better blast performance is observed for the nacre-like plates when compared to the bulk plates of same thickness. This better performance is measured in terms of the reduction in both the peak velocity and maximum deflection of the centre of back face for the 3.3-mm thick nacre-like plate, in addition to the increase of the load required to initiate cracking for both 3.3 and 5.5-mm thick nacre-like plates. These findings show that nacre-like plates can potentially reduce the threat of high velocity flying fragments at the back face that could be generated due to localised blast loading at the front face. This is achieved by the waviness of bonded layers that leads to the absorption of blast energy through delamination and friction, in addition to plastic deformation of layers. This is the key to reducing kinetic energy and/or increasing the blast resistance of the nacre-like plates.

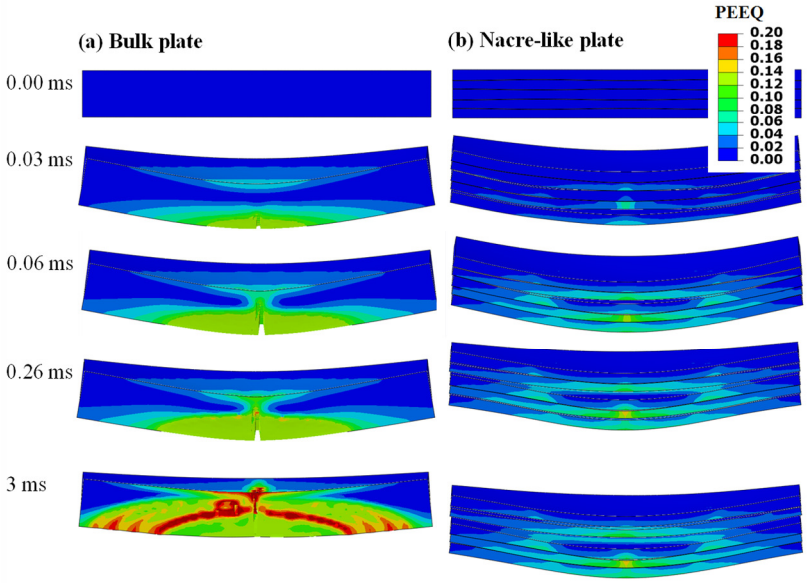

Fig. 9 Deformation process of 5.4-mm thick AA 7075 plates subjected to an impulsive load of 8 Ns: (a) Bulk plate; (b) Nacre-like plate.

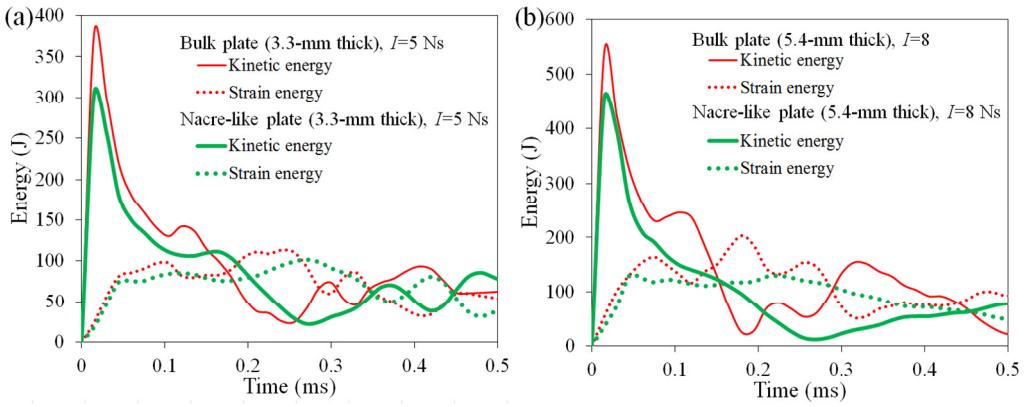

Fig. 10 Time histories of the energies in (a) 3.3-mm thick plates and (b) 5.4-mm thick plates.

The numerical model developed in this research could be used for the design of experimental testing by reducing the number of necessary tests and minimising necessary resources. We also acknowledge that more research has to be carried out to further support the findings in this study and to fully understand these types of bioinspired composite plates against blast loading since there have been few studies addressing these issues. In particular, for the experimental validation, nacre-like composites are the subject of our ongoing study and three-dimensional printing techniques could be employed to obtain nacre-like plates with wavy layering for high strain-rate tests.

4 SUMMARY AND CONCLUSIONS

A numerical investigation of the blast performance of bioinspired nacre-like plates and bulk plates was conducted. The composite, inspired by the hierarchical structure of nacre, was made of wavy layers of aluminium alloy AA 7075 bonded with toughened epoxy resin. The epoxy material was modelled using a user-defined interface cohesive element with both strength and toughness enhancements under compression, compared to their tensile counterparts. Composite and bulk plates with thicknesses of 3.3-mm and 5.4-mm were studied. A performance improvement compared to bulk plates was recorded for the nacre-like plates, which required larger loads to reach the onset of failure when compared to the same thickness bulk plate. In addition, a reduction of the peak velocity and maximum deflection of the back face was significantly observed for the 3.3-mm thick nacre-like plates. This better performance of the nacre-like plates is explained by the hierarchical structure facilitating a globalized energy absorption by inter-layered interlocking and delamination. It is concluded that the proposed bioinspired nacre-like plates are an interesting option for protective structures against localised blast loads. Further numerical and experimental works are still needed to reinforce and further support the findings in this study.

ACKNOWLEDGEMENTS

This work was supported in part by the Australian Research Council through Centre of Excellence for Design in Light Metals (CE0561574) and Discovery Projects (DP140100945 and DP1093485), and the National Natural Science Foundation of China (No. 11232003).

REFERENCES

[1] Zaera R. Ballistic Impacts on Polymer Matrix Composites, Composite Armor, Personal Armor
In: Abrate S, editor. Impact Engineering of Composite Structures, vol. 526: Springer Vienna; 2011. p. 305-403.
[2] Qi C, Yang S, Yang L-J, Wei Z-Y, Lu Z-H. Blast resistance and multi-objective optimization of aluminum foam-cored sandwich panels. Compos Struc 2013;105(0):45-57.
[3] Barthelat F. Biomimetics for next generation materials. Philos Trans R Soc A 2007;365(1861):2907-2919.
[4] Lei HJ, Zhang ZQ, Han F, Liu B, Zhang YW, Gao HJ. Elastic Bounds of Bioinspired Nanocomposites. J Appl Mech 2013;80(6):061017-061017.
[5] Espinosa HD, Rim JE, Barthelat F, Buehler MJ. Merger of structure and material in nacre and bone – Perspectives on de novo biomimetic materials. Prog Mater Sci 2009;54(8):1059-1100.
[6] Chen P-Y, McKittrick J, Meyers MA. Biological materials: Functional adaptations and bioinspired designs. Prog Mater Sci 2012;57(8):1492-1704.
[7] Meyers MA, Chen P-Y, Lin AY-M, Seki Y. Biological materials: Structure and mechanical properties. Prog Mater Sci 2008;53(1):1-206.
[8] Zhang ZQ, Liu B, Huang Y, Hwang KC, Gao H. Mechanical properties of unidirectional nanocomposites with non-uniformly or randomly staggered platelet distribution. J Mech Phys Solids 2010;58(10):1646-1660.
[9] Rim JE, Zavattieri P, Juster A, Espinosa HD. Dimensional analysis and parametric studies for designing artificial nacre. J Mech Behav Biomed Mater 2011;4(2):190-211.
[10] Hideki K, Taro S. The toughening mechanism of nacre and structural materials inspired by nacre. Sci Technol Adv Mater 2011;12(6):064710.
[11] Sun J, Bhushan B. Hierarchical structure and mechanical properties of nacre: a review. RSC Adv 2012;2(20):7617-7632.
[12] Barthelat F, Zhu D. A novel biomimetic material duplicating the structure and mechanics of natural nacre. J Mater Res 2011;26(10):1203-1215.
[13] Barthelat F, Tang H, Zavattieri PD, Li CM, Espinosa HD. On the mechanics of mother-of-pearl: A key feature in the material hierarchical structure. J Mech Phys Solids 2007;55(2):306-337.
[14] Humburg H, Zhu D, Beznia S, Barthelat F. Bio-inspired tapered fibers for composites with superior toughness. Compos Sci Technol 2012;72(9):1012-1019.
[15] Yao H, Song Z, Xu Z, Gao H. Cracks fail to intensify stress in nacreous composites. Compos Sci Technol 2013;81:24-29.
[16] Huang Z, Li H, Pan Z, Wei Q, Chao YJ, Li X. Uncovering high-strain rate protection mechanism in nacre. Sci Rep 2011;1:148.
[17] Knipprath C, Bond IP, Trask RS. Biologically inspired crack delocalization in a high strain-rate environment. J R Soc Interface 2012;9(69):665-676.
[18] Flores-Johnson EA, Shen L, Guiamatsia I, Nguyen GD. Numerical investigation of the impact behaviour of bioinspired nacre-like aluminium composite plates. Compos Sci Technol 2014;96:13-22.

[19] Tran P, Ngo TD, Mendis P. Bio-inspired composite structures subjected to underwater impulsive loading. Comput Mater Sci 2014;82(0):134-139.
[20] Abaqus Analysis User's Manual (Version 6.11), SIMULIA.2011.
[21] Johnson GR, Cook WH. A constitutive model and data for metals subjected to large strains, high strain rates and high temperatures. Proceedings of the 7th International Symposium on Ballistics, The Hague, The Netherlands1983. p. 541-547.
[22] Johnson GR, Cook WH. Fracture characteristics of three metals subjected to various strains, strain rates, temperatures and pressures. Eng Fract Mech 1985;21(1):31-48.
[23] Guiamatsia I, Nguyen GD. A thermodynamics-based cohesive model for interface debonding and friction. Int J Solids Struct 2014;51(3-4):647-659.
[24] Flores-Johnson EA, Saleh M, Edwards L. Ballistic performance of multi-layered metallic plates impacted by a 7.62-mm APM2 projectile. Int J Impact Eng 2011;38(12):1022-1032.
[25] Flores-Johnson EA, Muránsky O, Hamelin CJ, Bendeich PJ, Edwards L. Numerical analysis of the effect of weld-induced residual stress and plastic damage on the ballistic performance of welded steel plate. Comput Mater Sci 2012;58:131-139.
[26] Børvik T, Hopperstad OS, Pedersen KO. Quasi-brittle fracture during structural impact of AA7075-T651 aluminium plates. Int J Impact Eng 2010;37(5):537-551.
[27] Brar NS, Joshi VS, Harris BW. Constitutive model constants for Al7075-T651 and Al7075-T6. AIP Conf Proc 2009;1195(1): 945–948.
[28] Dorogoy A, Karp B, Rittel D. A Shear Compression Disk Specimen with Controlled Stress Triaxiality under Quasi-Static Loading. Exp Mech 2011;51(9):1545-1557.
[29] Wang RX, Shayganpur A, Sareskani S, Spelt JK. Analytical Peel Load Prediction as a Function of Adhesive Stress Concentration. J Adhes 2006;82(1):39-61.
[30] Langdon GS, Lemanski SL, Nurick GN, Simmons MC, Cantwell WJ, Schleyer GK. Behaviour of fibre–metal laminates subjected to localised blast loading: Part I—Experimental observations. Int J Impact Eng 2007;34(7):1202-1222.
[31] Yazici M, Wright J, Bertin D, Shukla A. Experimental and numerical study of foam filled corrugated core steel sandwich structures subjected to blast loading. Compos Struct 2014;110(0):98-109.
[32] Karagiozova D, Langdon GS, Nurick GN, Chung Kim Yuen S. Simulation of the response of fibre–metal laminates to localised blast loading. Int J Impact Eng 2010;37(6):766-782.
[33] Vo TP, Guan ZW, Cantwell WJ, Schleyer GK. Low-impulse blast behaviour of fibre-metal laminates. Compos Struct 2012;94(3):954-965.
[34] Vo TP, Guan ZW, Cantwell WJ, Schleyer GK. Modelling of the low-impulse blast behaviour of fibre–metal laminates based on different aluminium alloys. Compos B Eng 2013;44(1):141-151.
[35] Bahei-El-Din YA, Dvorak GJ, Fredricksen OJ. A blast-tolerant sandwich plate design with a polyurea interlayer. Int J Solids Struc 2006;43(25–26):7644-7658.